THE ARCHIVE OF MECHANICAL ENGINEERING

Vol. XLIX 2002 Number 3

Key words: *transonic flows, nonstationary airfoil loading*

WITOLD C. SELEROWICZ[*)]

TRANSONIC AIRFOIL FLOW INDUCED BY DAMPED OSCILLATIONS OF THE MAIN FLOW

A flow around an NACA0012 airfoil at special transonic flow conditions, characterised by damped oscillations of the main flow velocity, was investigated experimentally. On the basic of pressure measurements and flow visualisation, the time depending airfoil loading was reconstructed. Results, presented for a wide range of angle of attack ($\alpha = 0 \div 10^{\circ}$), show that during the excitation the normal aerodynamic force behaviour significantly differs from that of quasi- steady conditions. The pressure distributions on the airfoil surface depend on Mach number of the main flow as well on the phase of oscillation (deceleration or acceleration of the main flow velocity). The influence of the air humidity on the pressure distribution, normal aerodynamic force and centre of pressure is also considered.

1. Introduction

Small fluctuations of the flow parameters in transonic flow regime can considerably affect the airfoil flow [1], [2]. The self- excited oscillation of the shock wave on the upper airfoil surface leads to unsteady airfoil loading and increase of noise generation [3].

Apart from natural excitation, the periodic shock wave motion on airfoils at transonic flow conditions can be induced by external excitation. The phenomenon was observed on oscillating airfoils [4] at steady background flow conditions, and confirmed in numerical studies [5], [6].

Similar displacement of the shock wave position were reported in the case of a flow around an airfoil at unsteady transonic conditions, which were caused by oscillatory variation of the main flow velocity. The effect of such external excitation on the separation process was first presented in a visualisation study [7]. Changes in airfoil loading, calculated from pressure measurements on the

[*)] *Warsaw University of Technology, Institute of Aeronautics and Applied Mechanics; ul. Nowowiejska 24, 00-665 Warsaw, Poland; E-mail: seler@meil.pw.edu.pl*

NACA0012 airfoil, are the subject of interest in [8]. It was shown that the amplitude of the loading remains constant in the case of small airfoil angle of attack, and increases rapidly with increasing frequency of the background flow oscillations in the case of high angles of attack. The amplitude reaches its highest value when the forced oscillation frequency approaches the natural buffet frequency.

The level of air humidity can also influence the shock instability phenomenon at transonic flow conditions. In relationship to NACA0012 airfoil, the problem was first investigated experimentally in the case of steady background flow [9] in typical cases of flow separation: the beginning of boundary layer separation, separation with shock oscillation and total separation without shock.

The oscillatory flow around an airfoil, caused by external periodic excitation, is also sensible to the air humidity. Results of such experimental investigations reported in [10] showed that the fluctuations of the aerodynamic force decrease with increasing air humidity in whole range of oscillation frequencies.

The other interesting, but not reported problem, is the influence of periodic disturbances with time decreasing amplitude on the transonic airfoil flow. The first question is how the airfoil flow responds to such a rapid change of the background flow velocity. The next one is the influence of air humidity. This is the subject of interest in the present work.

2. Experimental set-up

The presented experiments were performed in a transonic wind tunnel of short operating time, shown schematically in Fig. 1. The air at atmospheric pressure is sucked from an elastic container to the vacuum vessel through the test section and controlled by the regulating valve (3). In all experiments air temperature in the container was 22°C, whereas the relative air humidity was varied in two steps: 14% (dry inlet air) and 60% (humid inlet air). During the tunnel operation the temperature of the air in the test section decreased. In contrary, the air humidity increased up to 40% in the first case and reached the overcooling vapour conditions in the second one. However, the condensation of the main stream was not observed, due to the short time of the expansion process in the tunnel test section.

Inside the test section, a symmetric NACA0012 airfoil with 120 mm chord length and 100 mm width was installed (1 in Fig. 1). It was specially prepared by assembling a set of 13 Kulite XCS pressure transducers, which were located inside the airfoil in the symmetry plane (Fig. 2). The transducers were placed on the upper (suction) surface only, because the former experiments [8] shown that the pressure changes on the airfoil bottom surface are, in relation to the upper surface, insignificant. Near the airfoil trailing edge an additional pressure transducer (number 14 in Fig. 2) was placed in the tunnel side wall.

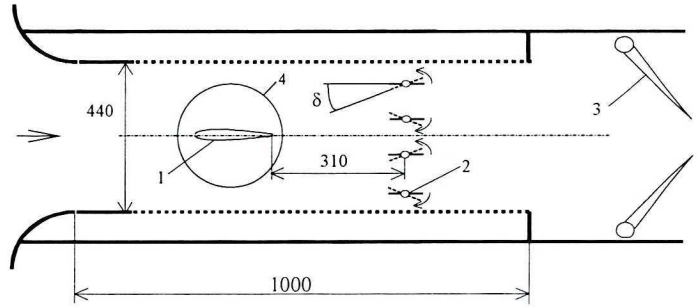

Fig. 1. Scheme of the transonic wind tunnel test section: 1 – NACA 0012 airfoil, 2 – set of four movable shutter, 3 – adjusting valve, 4 – glass window used in flow visualization

During the flow visualisation an another NACA0012 airfoil was assembled between two glass windows (4) of 230 mm diameter (see Fig. 1).

The airfoil angle of attack varied between $\alpha = 0^{\circ}$ and $\alpha = 10^{\circ}$. The Reynolds number, based on the tunnel velocity and chord length, changed from 2×10^{6} up to 1.7×10^{6} for initial and final tunnel operating conditions, respectively.

The fading disturbances of the tunnel main flow were produced using a set of four rectangular plates (2 in Fig. 1) installed downstream of the airfoil, 310 mm from its trailing edge. At the beginning of the experiment, all plates were positioned parallel to the tunnel axis. After the flow in the tunnel reached the operating conditions, all plates were rapidly turned round in directions shown schematically in Fig. 1. This caused the choking of the tunnel main flow and, in consequence, a decrease of the flow Mach number. After a few subsequent reflections from the tunnel inlet and, on the opposite side, from the controlling valve, the disturbances disappeared and the tunnel main flow reached its final steady conditions, which were characterised by a lower Mach number as at the beginning of the process.

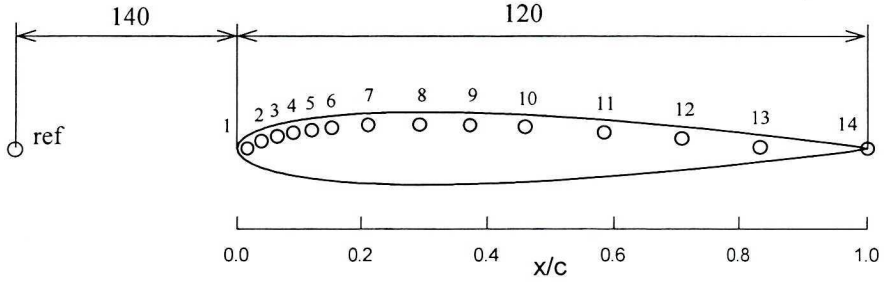

Fig. 2 Distribution of pressure transducers along the airfoil

Variation of the tunnel Mach number obtained at the reference point is shown in Fig. 3a. As it can be seen, the Mach number at the initial condition is equal to 0.72 and at final condition M=0.60. Between initial and final conditions three significant and four faint negative peaks of fading Mach number oscillation are noticeable. In each cycle of Mach number variation, five characteristic instances can be distinguished (Fig. 3a): initial conditions (i),

phase of maximum deceleration (ii), minimum M_{ref} (iii), maximum acceleration (iv) and maximum Mach number after acceleration (v).

In Fig. 3a an additional non-dimensional t/T axis is shown. It begins a short time before the fading oscillation starts. The time T, used for normalisation, equals 0.15s. Thus, the non-dimensional period t/T=1 contains the most important part of the considered phenomenon.

Mach number derivative as a function of time, calculated from Mach number variation, is shown in Fig. 3b. The extreme values of dM/dt occurred during the first oscillation cycle. They reached a value of -22 s^{-1} in the deceleration phase and +12 s^{-1} in the acceleration phase.

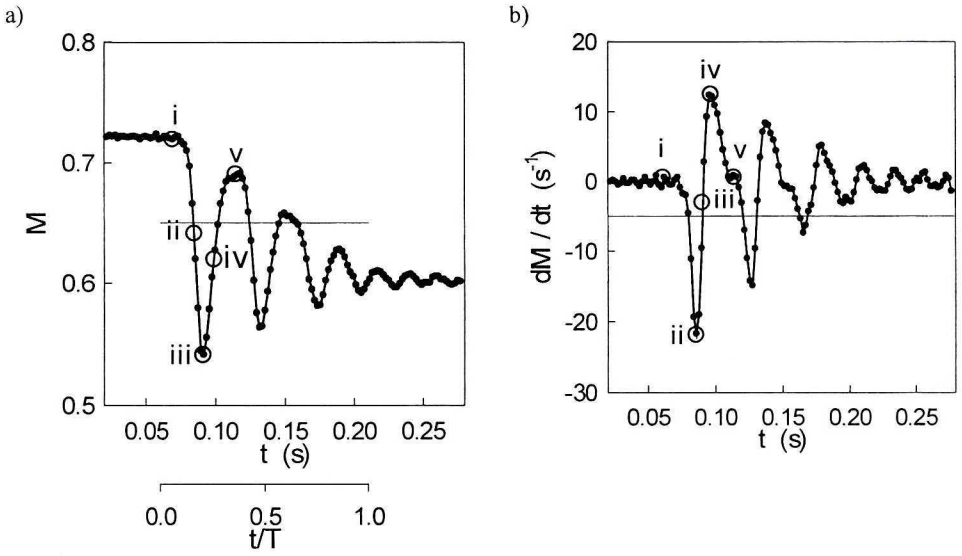

Fig. 3. Variation of Mach number at reference point (a) and Mach number derivative (b). t/T values are: 0.05 (i), 0.15 (ii), 0.20 (iii), 0.25 (iv) and 0.35 (v).

3. Airfoil loading

Pressure signals, recorded on the airfoil upper surface, facilitated the calculation of the momentary airfoil loading in form of the pressure coefficient disstribution. The value of C_p was determined from the formula

$$C_p = \frac{p - p_{ref}}{\frac{1}{2}\rho_{ref} u_{ref}^2} = \frac{\frac{p}{p_{ref}} - 1}{\frac{1}{2} k M_{ref}^2}$$

where: C_p – time depending pressure coefficient,

p – time depending pressure on the airfoil upper surface,

p_{ref}, ρ_{ref}, u_{ref} – time depending pressure, density and velocity at the reference point,

M_{ref} – time depending Mach number at the reference point (calculated from the isentropic formula),

k – isentropic exponent.

The presented final form of the pressure coefficient was obtained using equation of state for ideal gas. This assumption was allowed in both cases of air humidity levels, due to the negligible value of the vapour density (ρ_v=0.003 kg/m^3 at air humidity 14% and ρ_v=0.012 kg/m^3 at air humidity 60%) in contrary to density of the gas (ρ_g=1.181 kg/m^3).

Momentary C_p distributions versus the chord length x/c are presented in Fig.4 for airfoil angle of attack from $\alpha = 0^\circ$ up to $\alpha = 10^\circ$. The important part of the fading oscillation is shown in the graphs, because the t/T axis is the same as in Fig. 3a. Time interval between two successive C_p distributions is Δt=4 ms.

As it can be seen from Fig. 4a (α=0°) and Fig. 4b (α=2°), the C_p distributions show similar behaviour at small airfoil angle of attack. At the beginning of the considered time period, the distributions seem to be similar and characteristic for the attached flow without distinctive shocks. At t/T=0.15, a decrease of the negative values of C_p in the front and central part of the airfoil is noticeable. It is accompanied by a rapid increase of the positive C_p value in the rear airfoil part, what points out that the flow is still attached to the airfoil. This distribution corresponds to the minimum M_{ref} value from Fig. 3a. With an increase of M_{ref} (t/T>0.2) the C_p distribution returns to the shape described at initial conditions. This fluctuations repeats four times with decreasing amplitude. At the end of the considered time period the C_p distributions differ only insignificantly one from the other.

At angle of attack α=4°, the first five momentary C_p distributions (representing the initial conditions) show a new shape. They denote the existence of the lambda shock in the front part of the airfoil. At t/T=0.15, corresponding to the rapid diminishing of the M_{ref} in Fig. 3a, the C_p distribution changes and shows a new shape. This structure is typical for the attached flow without shocks waves. At t/T=0.3 the C_p distribution shows again a shape typical for the attached flow with a shock wave. However, this time the shock seems to be located closer to the airfoil leading edge. At the t/T=0.8, the shapes of C_p distributions denotes the attached flow with weak shock wave and subsequent separation (nearly linear increase of the C_p coefficient from the leading edge to the airfoil trailing edge).

The C_p distributions at α=6° show to be approximately the same as at α=4°. The main difference is that two next distinct flow phases of the attached flow with a shock wave (except the initial phase) can be now distinguished at t/T=0.35 and t/T=0.65. These distributions correspond to the maximum value of M_{ref} (see Fig. 3). At time instants corresponding to the maximum negative value of dM/dT (t/T=0.2 and t/T=0.5), pressure distributions denote an attached flow with very weak shocks (shocketts). At the end of the time period under consideration, the C_p distributions are typical for the attached flow with a weak shock.

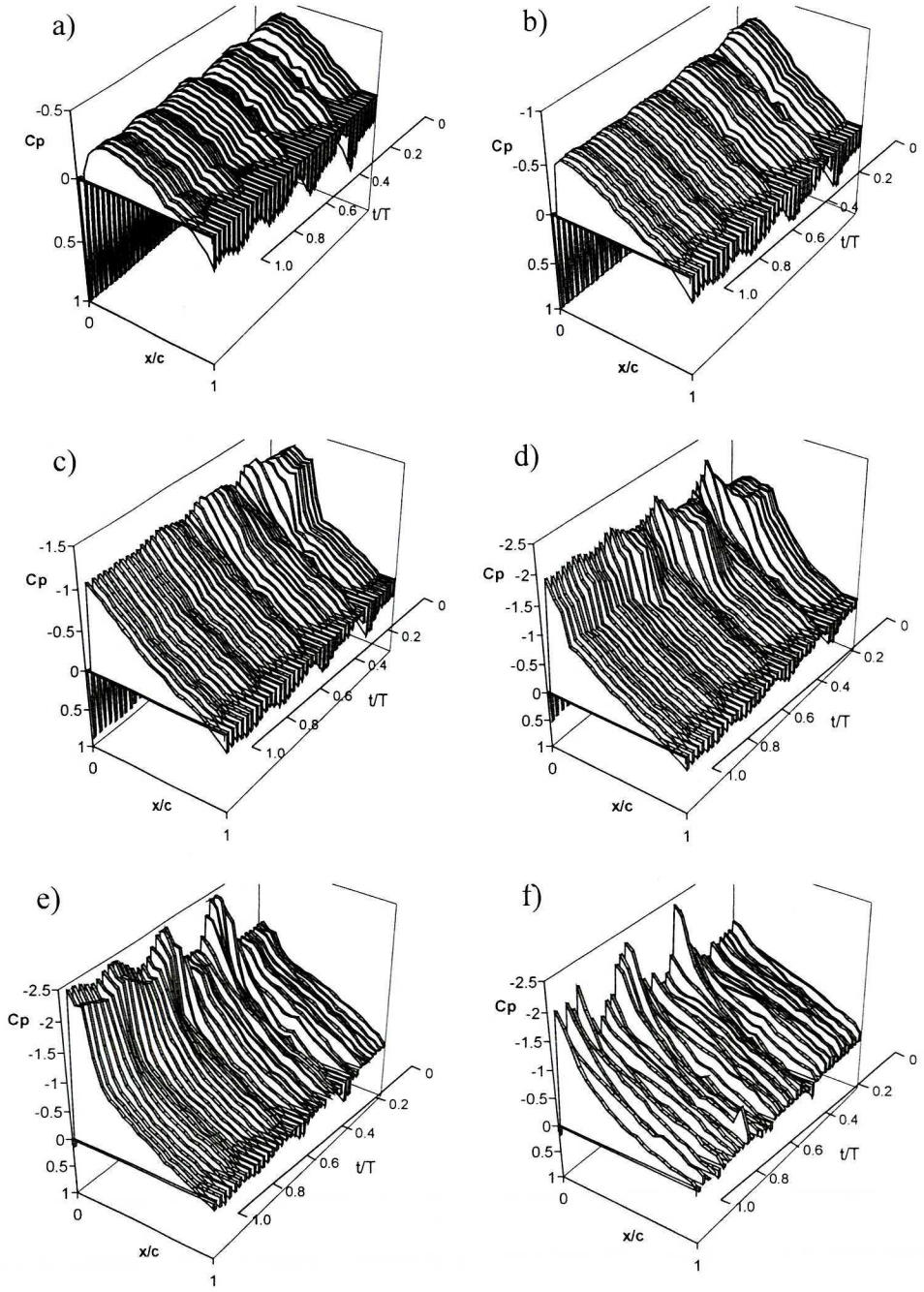

Fig. 4. Momentary pressure distributions on the airfoil upper surface for dry air (inlet humidity H=14%). Values of angle of attack α are: 0° (a); 2° (b); 4° (c); 6° (d); 8° (e) and 10° (f).

Histories of the C_p distributions received at α=8° show more intensive changes as than those described in the case of α=6°. In the initial phase, the C_p shapes are not identical. This is due to the fact that, at α=8° and M=0.72, strong self-exited oscillation of the shock wave and separation point occur on the upper airfoil surface. With decreasing of the mainflow Mach number (t/T>0.15), the C_p distribution rapidly changes and, in the flow phase, corresponding to the minimum value of M_{ref} (t/T=0.2) is characterised by maximum negative value of C_p near the airfoil nose and the positive C_p value at the trailing edge. In this flow phase, a set of very weak shock waves exists near the airfoil leading edge. Beyond these shocks, the flow is attacked to the airfoil.

Particular differences in C_p distributions are visible at α=10°. Distributions are not equal in the initial phase that denotes the unsteady flow conditions. In the next phase, a distinctive peak of negative C_p values at t/T=0.35, indicating an attached flow without separation, is visible. The same pressure shape occurs at t/T=0.6. In the final phase (t/T>0.8) C_p distributions show strong differences but still denote an attached flow. This indicates that, at final flow conditions, the oscillation of the airfoil flow occur.

Time depending aerodynamic force coefficient (component for suction surface only) was calculated from pressure distributions showed in Fig. 4, following the formula

$$C_n(t) = -\int_0^1 C_{p_u}(t)d\left(x/c\right)$$

where: $C_n(t)$ – time depending aerodynamic force coefficient,

$C_{p_u}(t)$ – temporary pressure coefficient at the upper airfoil surface,

x/c – non-dimensional cord length.

Results of numerical reconstruction are presented in Fig. 5 for various airfoil angle of attack α. As it can be seen, the $C_n(t)$ traces are similar to the $M_{ref}(t)$ trace shown in Fig. 3a, but not identical. Generally, up to five C_n minimum and four C_n maximum peaks can be distinguished on each $C_n(t)$ trace. In Fig. 5a, characteristic instants (i÷v), described in Fig. 3a, are also shown.

Initial parts (i) of the C_n traces (Fig. 5a, 5b and 5c), corresponding to initial conditions at α=0°, α=2° and α=4° are characterised by time invariably values of C_n. This denotes steady flow in these conditions.

At α=6°, 8° and 10°, the C_n values indicates loading fluctuations in the initial flow phase. They are relatively small at α=6° and distinctive at α=8° and 10°. As mentioned above, they result of self-exited airfoil oscillations (buffet). Strong disturbances in $C_n(t)$ can be seen at α=10° also in the final stage of considered time period. They are caused by flow oscillations, too. The minimum of the aerodynamic force C_n (instant ii) corresponds to the flow phase of maximum negative value of dM/dt (see Fig. 3a). The C_n values representing the first C_n maximum after acceleration phase (iv) are higher at α=0°,2° and 10° than C_n values representing the initial conditions, although the reference Mach number

corresponding to this flow phase (instant iv in Fig. 3a) is lower then M_{ref} at initial conditions (i). This phenomenon will be explained below. The instant corresponding to the first maximum of M_{ref} after acceleration phase (v) is characterised by distinctly lower value of C_n then in phase (iv) and a little lower then in phase (i). This denotes that in this flow phase new quasi-steady conditions are achieved, what is confirmed by M_{ref} trace shown in Fig. 3a.

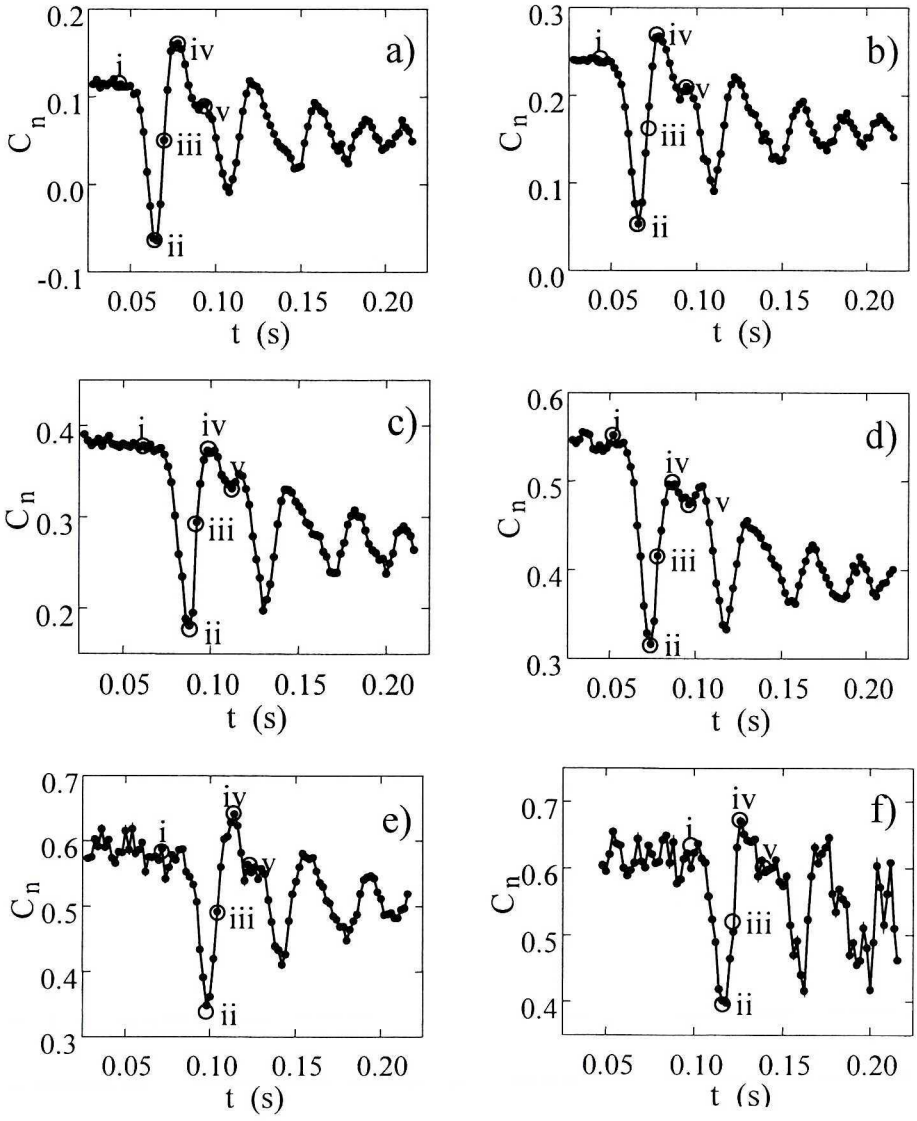

Fig. 5. Time histories of normal aerodynamic force coefficient C_n for dry air (inlet humidity H=14%). Values of angle of attack α are: 0° (a); 2° (b), 4° (c), 6° (d), 8° (e) and 10° (f). t/T values are: 0.05 (i), 0.15 (ii), 0.20 (iii), 0.25 (iv) and 0.35 (v)

A new representation of the calculated data is given in Fig. 6a÷6f. In these graphs, the aerodynamic force C_n is plotted versus momentary mainflow Mach number M_{ref} (the same as shown in Fig. 3a). As before, in Fig. 6a five characteristic instants i÷v (the same as in Fig. 3a and Fig. 5a) are also shown. As it can be seen from the plots, each C_n trace assumes a spiral shape, starting at initial conditions and ending at the final flow conditions. These shapes significantly differ from linear or nearly linear behaviour, which characterises the $C_n(M)$ dependence in steady flow conditions.

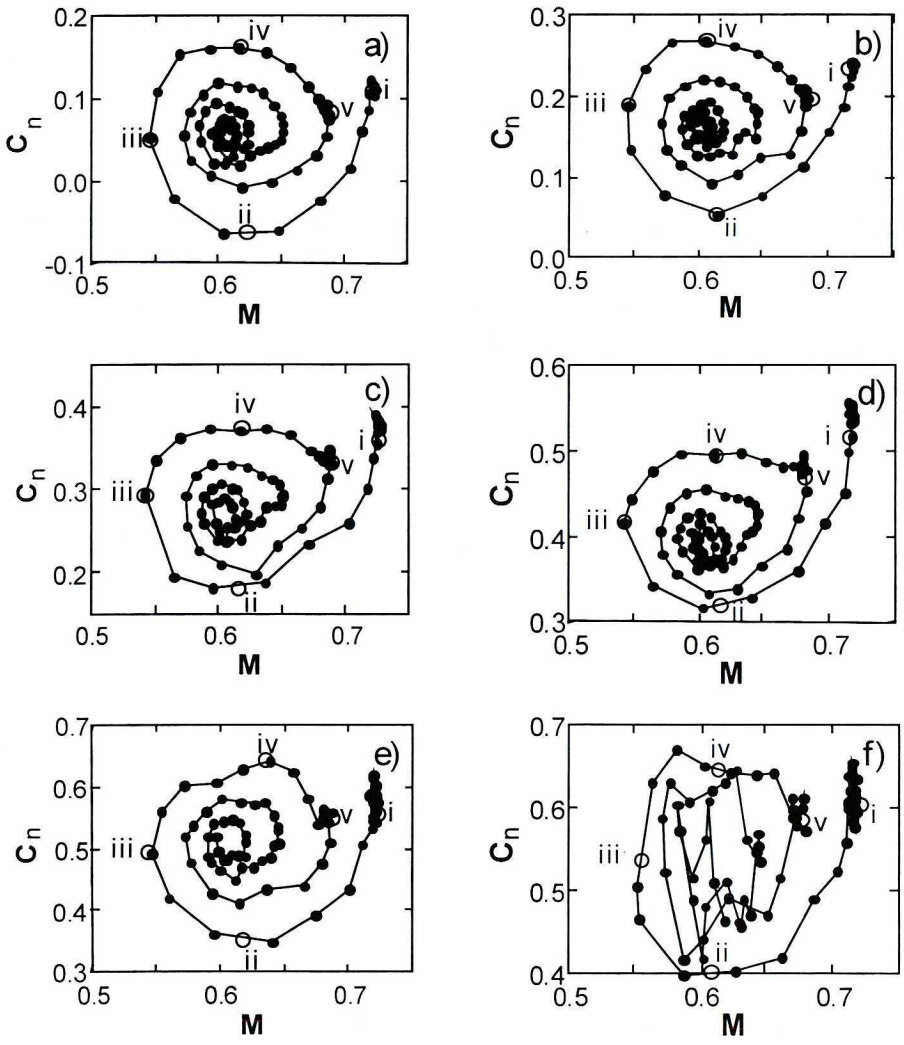

Fig. 6. Normal aerodynamic force coefficient C_n for dry air (inlet humidity H=14%) versus main flow Mach number. Values of angle of attack α are: 0° (a); 2° (b), 4° (c), 6° (d), 8° (e) and 10° (f). t/T values are: 0.05 (i), 0.15 (ii), 0.20 (iii), 0.25 (iv) and 0.35 (v).

The greater differences between the considered C_n values and values representing steady flow conditions are observed at Mach numbers corresponding to maximum (negative and positive) values of dM/dt (points i and iv). Such conditions occur, as it can be seen from Fig. 3b, in the middle of the deceleration and acceleration flow phase. With increasing time, the amplitude of the reference Mach number decreases, and the spiral shape of C_n narrows, until the value representing steady final conditions is achieved.

The described $C_n(M)$ behaviour remains unchanged for the angle of attack from α=0° to α=8°. At α=9° and α=10°, the spiral is not better visible, due to the C_n oscillations in the final flow phase.

Various C_n values, observed at the same reference Mach number M_{ref} in Fig. 6, result from various pressure distributions on the airfoil surface. This phenomenon is displayed in detail in Fig. 7. It shows the C_p distributions at constant flow Mach number in characteristic stages of the flow (t_1,t_2,t_3 and t_4). They are compared with C_p distribution representing steady flow (final conditions). As it can be seen, in the deceleration phase of Mach number changes (t_1), the C_p distributions attains greater values then at steady conditions, whereas in the acceleration phase (t_2) the obtained C_p values are lower (note the decreasing C_p scale). With increasing time, the differences in C_p distributions decrease and finally disappear, reaching a value representing the steady final conditions.

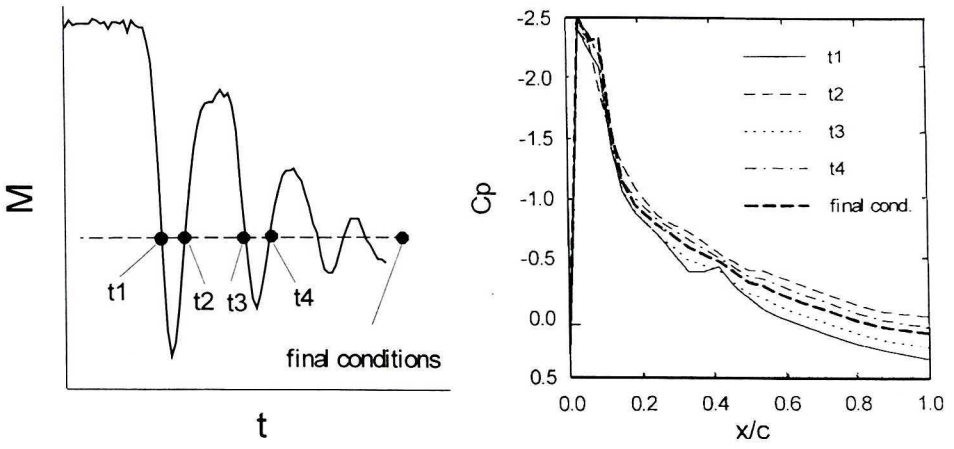

Fig. 7. Comparison of momentary pressure distributions for decelaration and acceleration flow phases. Inlet humidity H=14 %, angle of attack α = 8°

Conclusions resulting from Fig. 6a÷6f are summarised in Fig. 8. It shows values of C_{nmin}, C_{nmax} and $\Delta C=C_{max}-C_{min}$ in function of α. For α lower than 6°, values of C_{nmax} and C_{nmin} increase linearly, whereas ΔC_n remains constant. For α>6°, C_{nmin} increases slower than for α<6°. In consequence, ΔC_n reaches higher values.

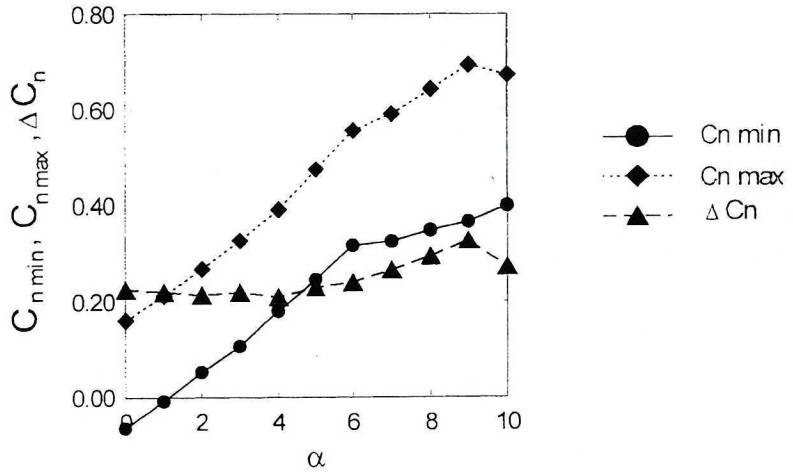

Fig. 8 Maximum and minimum values of the normal aerodynamic force C_n versus airfoil angle of attack

Parallel to the changes of the normal aerodynamic force, changes of position of the centre of pressure (point of intersection of the aerodynamic force with the airfoil chord) were observed. Two characteristic traces for α=6° and α=10° are presented in Fig. 9a and 9b. In the first case , which is typical for the airfoil flow without total separation, the changes of X_{Cn} are regular and in good correlation with the C_n changes. X_{Cn} values differ from 0 by up to 0.27. The first value corresponds to the flow phase with maximum negative value of *dM/dt* in main flow whereas the highest- with the highest positive value of *dM/dt*. In case of a fully separated flow (Fig. 9b) the changes are smaller and highly unregular. Only in the first phase of M_{ref} decrease, the decrease of X_{Cn} can be considered as regular.

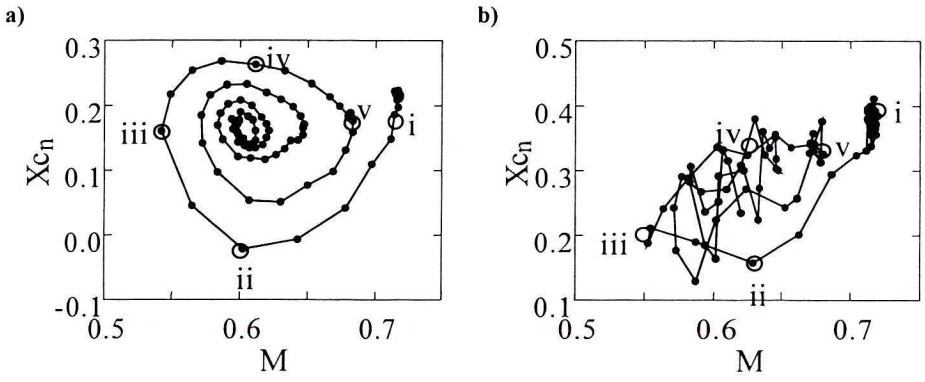

Fig. 9. Location of the centre of pressure versus mainflow Mach number. Inlet humidity H=14%, angle of attack: α = 6° (a) and α = 8° (b), t/T values are: 0.05 (i), 0.15 (ii), 0.20 (iii), 0.25 (iv) and 0.35 (v)

4. Effect of air humidity

The comparison of pressure distributions on the airfoil upper surface for dry (inlet humidity H=14%) and humid air (inlet humidity H=60%) is given in Fig. 10. The time instants shown in the graph represent the initial conditions (i), the moment of minimum dM/dt value in the deceleration phase (ii), the instant

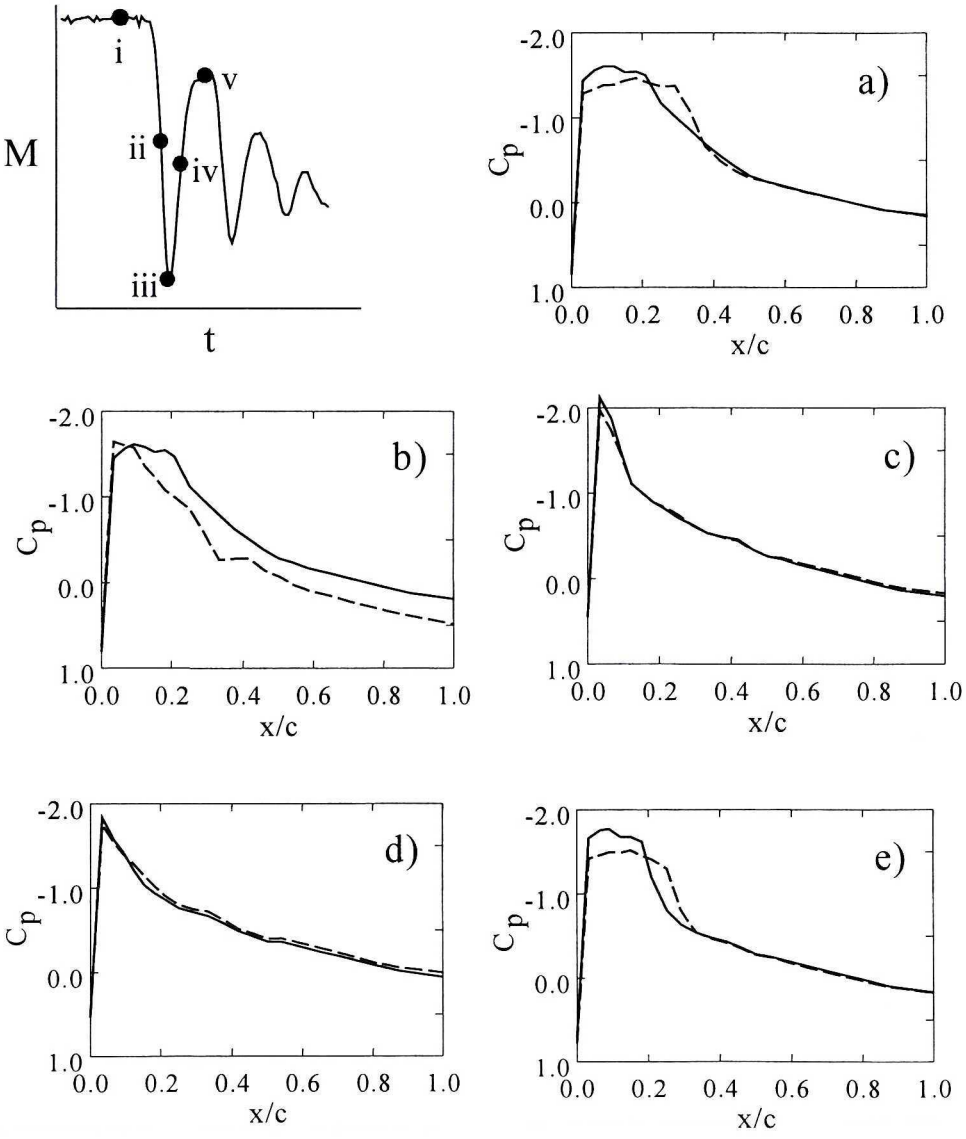

Fig. 10. Comparison of pressure distributions on airfoil upper surface in characteristic instants for dry (inlet humidity H=14 % - continuous lines) and humid air (inlet humidity H=60 % - dashed lines). Angle of attack $\alpha = 6^{\circ}$. t/T values are: 0.05 (i), 0.15 (ii), 0.20 (iii), 0.25 (iv) and 0.35 (v)

of minimum mainflow Mach number (iii), the instant of maximum dM/dt in the acceleration phase (iv) and finally the maximum M_{ref} after the first oscillation cycle (v). The corresponding results of flow visualisation obtained by the Schlieren method with spark light source (exposure time 1 μs) are presented in Fig. 11 for both dry (left column) and humid air (right column).

The pressure distributions shown in Fig. 10a, representing the initial conditions (i), are typical for the flow with shock wave of lambda type. The moment of rapid pressure increase denotes that the shock in the case of a humid air is located further away from the leading edge than for dry air. In the rear parts of the airfoil($x/c>0.4$) the pressure distributions are identical. Photographs shown in Fig. 11a confirm these conclusions. The picture for a dry air (at the left) indicates the presence, behind the shock of lambda type, a group of upstream moving waves. They are originating at the trailing edge and associated with boundary layer fluctuations due to unsteady shock motions [11]. In oscillation phase, shown in the picture, the boundary layer seems to be separated just from the airfoil nose. For the humid air (right picture), as also denoted by pressure distributions, the shock is located further from the airfoil nose. It is preceded by a set of two condensation regions similar in shape to the shock. The boundary layer is now thinner than in the case of dry air and attached to the airfoil. Despite different pressure distributions, the aerodynamic force coefficients C_n achieve, in both cases, practically identical values (Fig. 14a). This can be also deduced directly from Fig. 10a.

Substantial differences in pressure distributions are also noticeable in the case of maximum M_{ref} deceleration (ii). For dry air the existance of a weak shock wave in the initial part of the airfoil (Fig. 11b) is confirmed by the pressure distribution (Fig. 10b), whereas only a much weaker shock nearer the airfoil nose can be assumed in the case of humid air. Behind the shock, the flow is attached to the airfoil. In consequence, on the whole airfoil upper surface the pressures are lower then those in the case of dry air. In consequence, the aerodynamic force coefficient C_n is higher for dry then for humid air. It is confirmed by Fig. 14a.

At the time instant corresponding to the minimum Mach number of the mainflow (iii), the pressure distributions (Fig. 10c) are identical and characteristic for the attached flow without shocks. This is confirmed by the photographs shown in Fig. 11c. Only a set of very weak shocks (shocklets) in the front part of the airfoil can be distinguished on both pictures. Due to such pressure distributions, the values of C_n (Fig. 14a) are identical.

The same situation can be observed at the maximum acceleration phase (instant iv) where the pressure distributions differ only insignificantly from one another. Due to the higher mainflow Mach number, two weak shocks of lambda type are visible on the airfoil (Fig. 11d). In the whole range of x/c, values of C_p for humid air are a little lower, what leads to a higher value of C_n (Fig. 14a).

At the instant (v), which represents the first maximum of the main flow Mach number after acceleration phase, essential differences are noticeable

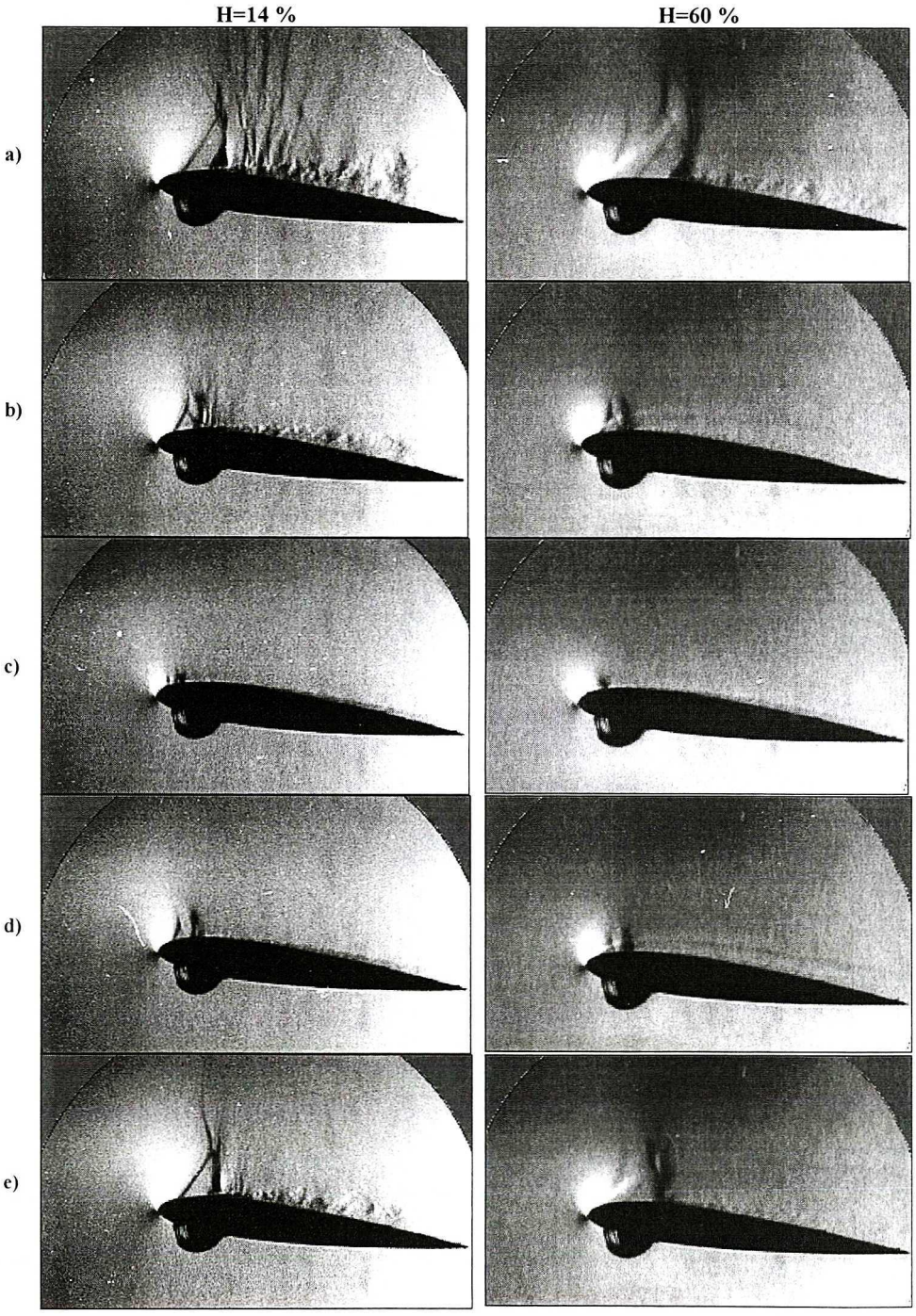

Fig. 11. Schlieren photographs of airfoil flow at $\alpha=6^{\circ}$ for dry (inlet humidity H=14% – left column) and humid air (inlet humidity H=60% – right column). For time instances see Fig. 10

again. As it was at instant (i), both pressure distributions (Fig. 10e) denote the existence of a shock followed by attached boundary layer. In the case of dry air (Fig. 11e – left column), the shock has a typical lambda shape and is located closer to the airfoil nose than for humid air. A turbulent boundary layer behind the shock is well visible. For the humid air (right column), the shock is of the same type, but is preceded by a weak condensation shock and situated a little further from the airfoil nose. As a consequence of such pressure distributions, different C_n values are obtained in Fig. 14a.

Pressure distributions and Schlieren photographs received at angle of attack α=8° are shown in Fig. 12 and Fig. 13. Time instants are the same as in the case of α=6°.

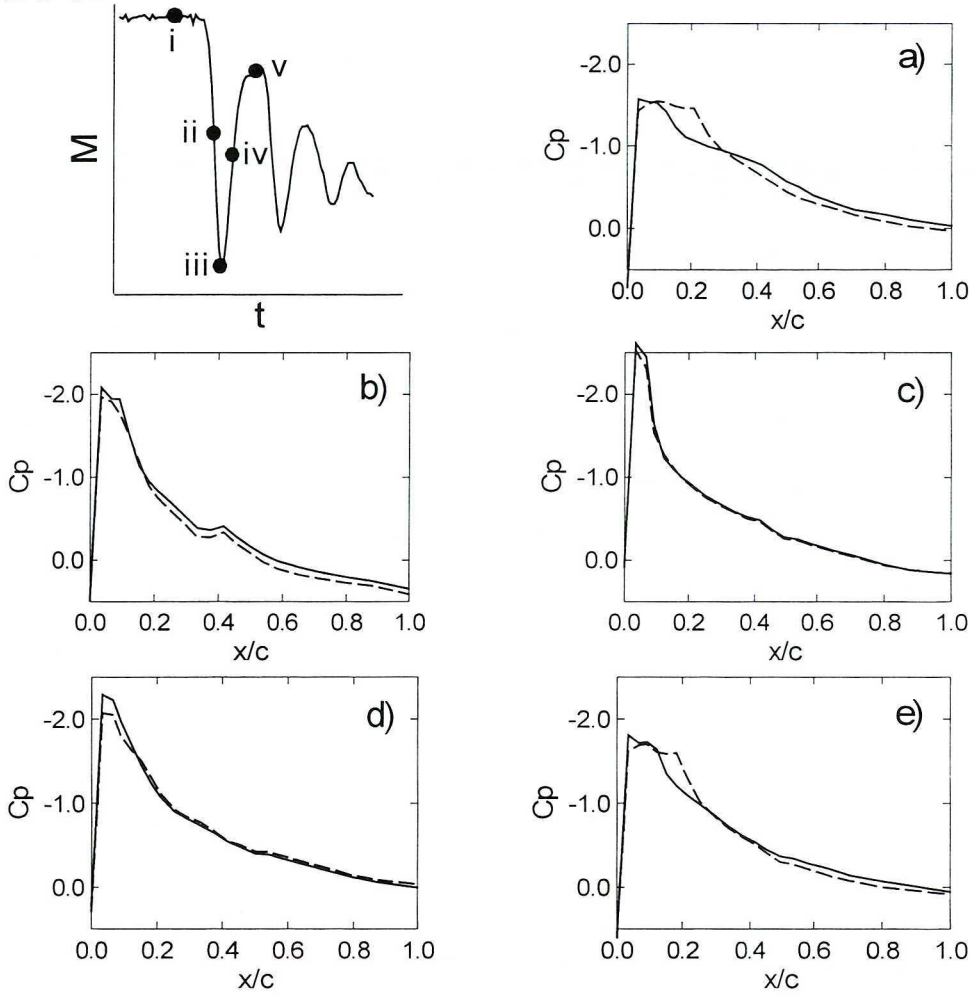

Fig. 12. Comparison of pressure distributions on airfoil upper surface in characteristic instants for dry (inlet humidity H=14% – continuous lines) and humid air (inlet humidity H=60% – dashed lines). Angle of attack α=8°. t/T values for successive pressure distributions are: 0.05 (a), 0.15 (b), 0.20 (c), 0.25 (d) and 0.35 (e)

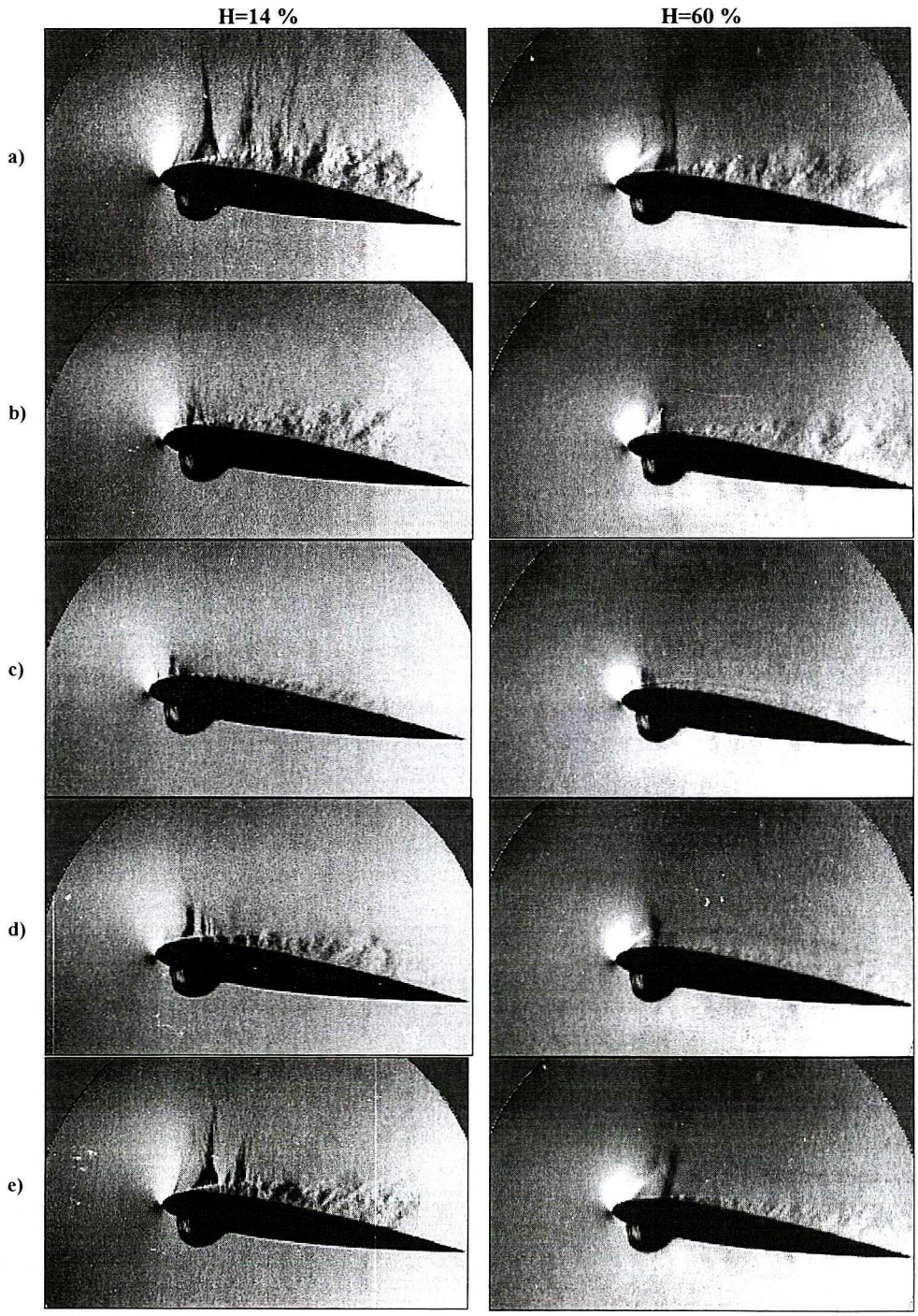

Fig. 13. Schlieren photographs of airfoil flow at α=8° for dry (inlet humidity H=14% – left column) and humid air (inlet humidity H=60% – right column). For time instances see Fig. 12

At the initial conditions (i), the flow for dry air is characterised by full separation, what is well visible in the first left picture (Fig. 13a). As in the case α=6°, behind the shock of lambda type a set of upstream moving waves and fluctuations of the separated boundary layer are visible. In the case of humid air (right picture), the area of full separation is a little smaller. This is due to the short region of attached flow, which can be seen in the initial part of the airfoil. On the airfoil nose, a rudimentary condensation shock can be distinguished. This situation is confirmed by pressure distributions presented in Fig. 12. In the front part of the airfoil, higher negative C_p values are obtained for humid air, as a consequence of the position of shock wave. The positive pressure gradient for $0.2<x/c<0.4$ is much smaller than for $0.1<x/c<0.2$, what is typical for separated flow. In rear part of the airfoil ($x/c\geq0.4$), pressure distribution for dry air is characterised by little higher negative C_p values. As it was at α=6°, both pressure distributions give the same C_n values, what is confirmed by Fig. 14b.

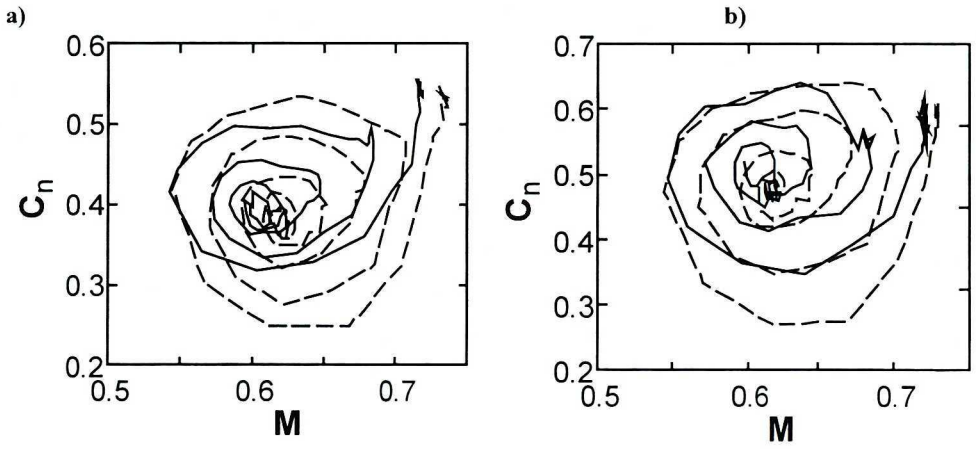

Fig. 14. Comparison of normal aerodynamic force coefficients C_n for dry (inlet humidity H=14% – continuous lines) and humid air (inlet humidity H=60% – dashed lines) at angle of attack α=6° (a) and α=8° (b)

At the instant of maximum deceleration (ii), weak shocks near the airfoil leading edge are visible for both dry and humid air (Fig. 13b). Only small differences can be recognised in the pressure distributions. The much higher positive pressure gradient in the front part of the airfoil ($x/c<0.4$) than that in the rear part ($x/c>0.4$) indicates that the flow is attached immediately behind the shock. Afterwards, the boundary layer separates. In consequence, the C_n value for dry air is higher than for humid air (Fig. 14b).

In the flow phase of minimum Mach number (iii) both pressure distributions (Fig. 12c) are identical for dry and humid air and typical for the flow without boundary layer separation. This situation is confirmed by Schlieren photographs (Fig. 13c). On the airfoil nose a set of rudimentary weak shocks (shockletts) are

visible. In the other airfoil part, the flow is attached. As a result of this situation, identical values of C_n in Fig. 14b are noticeable for minimum value of M_{ref}.

In the phase of maximum acceleration (Fig. 12d), both pressure distributions show similar shapes. In comparison with instant (iii), the minimum C_p values are now lower, and the pressures at the airfoil trailing edge do not achieve positive values. This indicates the possibility of flow separation. Photographs of flow (Fig. 13d) confirm this situation, especially for dry air.

In the flow phase of maximum Mach number after acceleration (v), the pressure distributions (Fig. 12e) and photographs (Fig. 13e) indicate again a flow with shock wave and flow separation. A different values of C_n result from this pressure distributions, what is confirmed in Fig. 14b.

Comparison of normal aerodynamic force coefficients for dry and humid air, in the whole considered time period, calculated in the same way as in chapter 3 and plotted versus main flow Mach number, is presented in Fig.14a (α=6°) and Fig. 14b (α=8°). In the case of humid air (dashed lines), one can note the same spiral character of C_n changes, as for dry air (continuous lines), although differences between maximum C_n and minimum C_n are much greater for humid air.

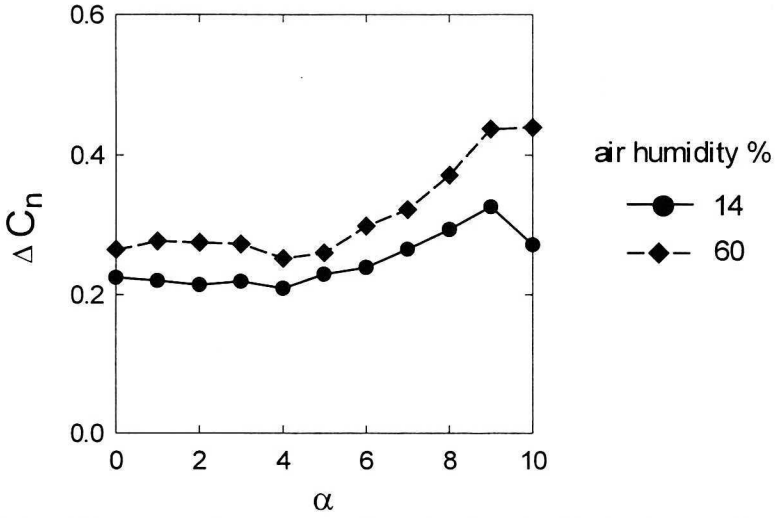

Fig. 15. Values of $\Delta C_n = C_{n\,max} - C_{n\,min}$ versus airfoil angle of attack α for dry (inlet humidity H=14% – continuous line) and humid air (inlet humidity H=60% – dashed line)

Values of $\Delta C_n = C_{nmax} - C_{nmin}$ for humid air and their comparison with the data for dry air are plotted in Fig. 15 versus angle of attack α. As it can be seen, in the whole range of α under consideration, values of ΔC_n for humid air are higher than for dry air. For airfoil angle of attack $\alpha = 0° \div 7°$ (steady flow at initial and final conditions) differences remain in the range of 25÷27% and increase up to 60% at α=10% (fully separated flow at initial conditions and flow with self exited oscillations at final conditions).

5. Conclusions

Strong damped oscillations of the background flow have a significant influence on the transonic airfoil flow. Due to the variation of the main velocity, the structure of the flow around the airfoil changes considerably, especially at higher angles of attack. In consequence, the flow patterns vary from fully attached to fully separated flow, accompanied by stronger or weaker shock waves. This leads to changes in pressure distributions, particularly on the upper airfoil surface, and finally to variation of normal aerodynamic force coefficient and centre of pressure.

During variation of the reference Mach number, the normal aerodynamic force coefficient C_n changes from initial to the final value in characteristic spiral form. The minimal value of C_n appears during velocity deceleration at the flow phase corresponding to the instant of minimum dM/dt. In contrary, the maximum C_n values were obtained at maximum dM/dt during acceleration flow phase. This C_n value shows to be generally higher than at initial conditions, although the Mach number is lower.

The amplitude of C_n variations keep nearly constant for angles of attack ≤ 6 and grows for higher values of the angle. The same behaviour as that observed in C_n is noted for the centre of pressure changes.

The humidity level of air also affects the variation of C_n with M. For all angles of attack under consideration, greater differences in aerodynamic force were observed for humid then for dry air. At steady initial and final flow conditions, differences in C_n with can be considered as negligible.

This work was financially supported by State Committee for Scientific Research in Poland (Project No 7 T07A 026 16).

Manuscript received by Editorial Board, January 31, 2002.

REFERENCES

[1] Mabey D. G.: Physical phenomena assotiated with unsteady transonic flows, in Unsteady transonic aerodynamics. Ed. D. Nixon, Progress in Astronautics and Aeronautics, Vol. 120, 1989, pp. 1÷56.

[2] Seegmiller H. L., Marvin J. G., Levy L. L.: Steady and unsteady transonic flow. AIAA Paper 78÷160, 1978.

[3] Mabey D. G.: Some aspects of aircraft dynamic loads due to flow separation., Progr. Aerospace Sci. 26, 1989, pp.115÷151.

[4] Davis S. S., Malcolm G. N.: Transonic shock- wave, boundary- layer interactions on an oscillating airfoil. A1AA J. Vol. 18, No.11, 1980, pp. 1306÷1312.

[5] Chyn W. J., Davis S. S.: Numerical studies of unsteady transonic flow over an oscillating airfoil. AGARD- 374, Paper 3 1984.

[6] Houwink R.: Unsteady airload computations for airfoils oscillating in attached and separated compressible flow'. Paper 14, AGARD-CP-386, 1985.

[7] Szumowski A.P.: Meier G.E.A.: Forced oscillations of airfoil flows, Experiments in Fluids 21, 1996, pp.457÷464.

[8] Selerowicz W. C., Szumowski A.P.: Airfoil flow instabilities induced by background flow oscillations. Experiments in Fluids, 2001.

[9] Nosal Z., Selerowicz W. C.: Separated transonic airfoil flow of humid air. Proc. Fourth Int. Sem. on RRDPAE_2000, pp.19÷24.

[10] Selerowicz W.C.: The effect of air humidity on oscillatory airfoil flow. Archiv of Mech. Eng., 2002, Vol. 1, pp. 47÷63.

[11] Lee B. H. K.: Oscillatory shock motion caused by transonic shock boundary-layer interaction. AIAA Journal, Vol. 28, 1990, No. 5, pp. 942÷944.

Transoniczny opływ profilu wywołany tłumionymi oscylacjami przepływu głównego

Streszczenie

W pracy badano na drodze doświadczalnej opływ profilu NACA0012 w specyficznych warunkach, wywołanych przez tłumione oscylacje przepływu głównego. Na podstawie pomiarów ciśnień oraz wizualizacji przepływu rekonstruowano zmienne w czasie obciążenia profilu. Wyniki badań, przeprowadzonych w szerokim zakresie kątów natarcia (α=0÷10°) wskazują, że podczas cyklu silnej oscylacji siła aerodynamiczna przyjmuje inne wartości niż podczas przebiegu quasi-ustalonego.